International Journal of Geo-Engineering

RESEARCH Open Access

Impact of dissolved salt type and content on mechanical and physical properties of porous cementitious materials

Mohammad Mehdi Karbala[1†], Soha Iranfar[2†], Mohammad Hossein Shahsavari[3] and Mahmood Shakiba[4*]

†Mohammad Mehdi Karbala and Soha Iranfar contributed equally to this work.

*Correspondence:
Mahmood Shakiba
mshakiba@um.ac.ir
[1]Rock Mechanics Division, School of Engineering, Tarbiat Modares University, Tehran, Iran
[2]Department of Petroleum Engineering, Abadan Faculty of Petroleum, Petroleum University of Technology (PUT), Abadan, Iran
[3]Department of Petroleum Engineering, Amirkabir University of Technology (Tehran Polytechnic), Tehran, Iran
[4]Department of Chemical Engineering, Faculty of Engineering, Ferdowsi University of Mashhad, Mashhad, Iran

Abstract

Salt precipitation is a major factor influencing the internal characteristics of concrete during curing. In this study, the impacts of the type and concentration of various salts on the characteristics of porous cementitious materials were investigated using a series of engineered porous concrete specimens. The results indicated that chemical interactions among interparticle cement, clay mineral, calcite, and different salts in aqueous media during 28 days of curing could alter properties such as porosity, permeability, and mechanical strength depending on salt concentration. Among these, concrete permeability was most affected. There was an inverse relationship between the content of monovalent ions and concrete porosity and permeability. In contrast, for divalent ions in the concentration range of 10–30 g/L, an optimum value of 15 g/L resulted in the lowest salt precipitation and highest porosity and permeability values. Furthermore, different salts present during curing led to an increase of up to 16% in compressional wave velocity. Based on the results of ultrasonic and uniaxial compressive strength (UCS) tests, linear and exponential correlations were observed between porosity and compressional/shear wave velocities, while UCS was exponentially related to porosity.

Highlights

- The effects of chemical interactions of various ions on concrete properties were investigated.
- The impacts of both monovalent and divalent ions on porosity and permeability were studied.
- Divalent ions have an optimum concentration of 15 g/L at which the least precipitation occurs.
- An increase in compression sonic wave velocity due to modifying concrete integrity was observed.

Keywords Salt precipitation, Curing process, Geochemistry, Mechanical and physical properties, Engineered porous concrete, Cementitious materials

Introduction

Salt precipitation significantly influences the microstructure and mechanical integrity of cementitious materials during curing. This phenomenon, which involves salt transport, crystallization, and pore filling, is relevant to various engineering applications including soil stabilization, concrete durability in saline environments, subsurface infrastructure performance, and underground formations. The underlying processes are driven by physicochemical interactions between pore water, cement phases, and external ions under varying environmental conditions [1–7]. This phenomenon naturally taking place at the pore scale at ambient and higher temperatures and pressures is greatly affected by the heterogeneity of the pore space morphology and pore size distribution (PSD) [8–11]. Large pores are the most likely places for salt crystals to grow and precipitate in porous materials. This is because growth in small pores necessitates a substantial increment in surface area relative to a slight increase in volume [12]. In this regard, saline water drying and evaporation, mineral replacement processes, and chemical reactions cause salt to precipitate, crystallize, and grow in concrete and soil in porous media [10]. It is worth mentioning that the permeability and porosity as the main physical properties of the porous concretes would be decreased by salt precipitation [9].

Literature review

Previous research has shown that salt crystallization can obstruct pore spaces, reduce permeability, and alter porosity distribution in cement-based materials. These effects are magnified in heterogeneous pore networks, where salts preferentially accumulate in larger or more accessible voids. Several studies have investigated salt-induced damage in natural rocks, such as sandstones and shales, particularly in the context of CO_2 injection or drying processes [13–17]. However, such studies primarily address long-term secondary property changes, which occur after material post-curing due to environmental exposure. In contrast, limited studies have focused on primary physical and mechanical characteristics such as porosity, permeability, and strength that evolve during the initial curing phase. Espinosa-Marzal and Scherer (2013) and Tang et al. (2015) reported that the various salts (NaCl, KCl, Na_2SO_4, and $MgSO_4$) and pore structure of the host rock had an impact on the pore-clogging caused by salt precipitation. According to their experimental outcomes, salt precipitation could reduce rock porosity and permeability by 14.6% and 83.3%, respectively. The experimental results also revealed that salt precipitation had a higher effect on pores with smaller diameters than on larger ones [18, 19]. Shokri-Kuehni et al. (2017) performed a series of experimental tests to investigate the effects of salinity and precipitation during brine evaporation in porous media. The results demonstrated that salt precipitation could be substantial, particularly while the brine was saturated with halite. The permeability may drop to 73% of its initial amount under such circumstances [20]. He et al. (2019) performed several pore-scale visualization experiments to investigate the morphology, distribution, and impact of salt deposition on reducing the permeability of porous structures. The results revealed that ex-situ precipitation could happen for hydrophilic and neutral porous surfaces and completely clogged pore throats and bodies, causing a considerable decrease in permeability. Besides, a decrease in permeability was observed due to raising the injection rate of CO_2 [21]. Zhang et al. (2020) investigated the effects of salt precipitation on the physical properties of a tight gas reservoir. Their findings showed that rock permeability was

reduced over time by more than 90% compared to initial conditions where the size of the salt crystal and the diameter of the pore throat were the same [22]. Zhang et al. (2022) studied the influence of salt precipitation on the secondary physical characteristics and the adsorption capacity of the shale matrix. The results demonstrated that porosity, permeability, and specific area of the shale matrix decreased by 23.0%, 47.0%, and 20.4%, respectively. Larger pores and throats were more affected by salt precipitation, which led to the breakdown of reservoir fluid flow channels and a significant shift in the distribution of pore sizes [23]. Yang et al. (2023) conducted a series of geo-mechanical tests to investigate the impact of two various brine solutions (5% sodium chloride and 5% potassium sulfate) on the mechanical, acoustic emission, and fracture characteristics of sandstone samples under various unloading conditions [24]. Almutairi et al. (2023) studied the effects of ion and temperature on mineral reactions and fine migration in carbonate structures. They noticed two distinct mineral reactions: mineral dissolution, leading to increased permeability and grain redistribution, and cation exchange, which facilitates the release of silicate particles [25]. Zeng et al. (2023) investigated the impact of fluid saturation and salinity on the mechanical characteristics of rocks using a novel triaxial compressional system incorporating micro-seismicity monitoring. The experiment involved conducting rock failure and fracture reactivation tests on dry and wet samples (i.e., saturated with brines) of varying salinity levels. The findings indicated that the peak stress of saturated specimens is lower than that of unsaturated specimens, providing evidence that fluid saturation might negatively impact rock strength [26]. Hosseini et al. (2024) created a theoretical framework to forecast the occurrence of formation damage due to the accumulation of salt deposits. A comprehensive model incorporating thermodynamics, kinetics, and hydrodynamics was established and integrated with the ion transport equation to depict the motion of ions accurately. The suggested model could precisely forecast the distribution of scale precipitation and the subsequent decrease in the porosity and permeability in a one-dimensional porous medium [27].

Study motivation and scope

To the best of the authors' knowledge, previous research has mainly focused on post-curing (secondary) effects of salt precipitation as a detrimental element under CO_2 injection, evaporation, or environmental exposure on the petrophysical properties of porous materials. However, limited studies have systematically investigated how various dissolved salts and their concentrations affect the primary microstructural and mechanical development of engineered porous cementitious materials during the curing process. In other words, most existing studies either neglect the curing phase or treat salt as a post-cure stressor. The current research fills this gap by experimentally examining the direct impact of monovalent and divalent ion interactions on salt precipitation patterns, pore structure modification, and strength development using engineered porous concrete samples. For this purpose, the reaction between the cement hydration process and various external salts, including sodium chloride, sodium sulfate, calcium chloride dihydrate, and magnesium chloride hexahydrate during curing time for the porous concretes comprehensively investigated by microstructural, mineralogical, physical, chemical, and mechanical analysis. The use of synthetic samples with controlled composition allows for an isolated evaluation of salt-specific effects, contributing novel insights into optimizing material formulation for enhanced performance in saline environments and designing

salt-tolerant cementitious materials for use in saline groundwater zones, subsurface formations, and other chemically aggressive environments. Moreover, the current research can draw a specific picture of primary chemical interactions to better understand the changes occurring over the curing period causing impairments in porous concrete properties.

Methodology workflow

This study employed a multi-method approach to assess the chemical, physical, and mechanical changes induced by salt interactions during concrete curing. The analytical techniques used include:

- X-ray Diffraction (XRD): To analyze the mineralogical changes and reaction products resulting from salt–cement interactions, XRD analysis was performed. The XRD measurements were conducted using Cu Kα radiation at 60 kV and 60 mA, 0.0310° step size over a 2θ range of 10°–70°. XRD spectra were obtained for samples corresponding to both the lowest (10 g/L) and highest (30 g/L) salt concentrations to capture the contrast in reactivity and phase formation. These measurements allowed for identification of crystalline compounds such as portlandite, ettringite, and various residual salts.
- Fourier-Transform Infrared Spectroscopy (FTIR): This test was accomplished to detect chemical bonding and molecular vibrations indicative of hydration and salt-related compounds. The test was performed in the range of 4000–400 cm^{-1} at 0.4 cm^{-1} resolution.
- Field Emission Scanning Electron Microscopy (FESEM): This test was performed to evaluate the microstructure, pore surface morphology, and elemental composition of precipitated crystals.
- Physical and mechanical tests: These include porosity and permeability measurements, compressional and shear wave velocity tests, and uniaxial compressive strength (UCS) testing, performed on dried and trimmed samples after 28 days of curing.

This comprehensive set of methods allows for correlating chemical reactions with changes in physical structure and mechanical performance.

Concrete constituents

Porous concrete samples used in the current study were artificially made of sand particles, kaolinite as a clay mineral, and Portland cement with a density of 3.11 g/cm^3. Concrete samples, owing to their analog chemical properties and uniform structural texture without any heterogeneities, have been widely used in rock, soil, and cementitious material studies [28–34]. To cover a broad particle size range, sand grain sizes maintained constant in the range of 0.1 to 0.8 mm (i.e., very fine to coarse type) with a 2.64 g/cm^3 density. The X-ray fluorescence spectrometry (XRF) analyses of the cement, sand grains, and kaolinite are given in Table 1.

Figure 1 illustrates the grain size distribution curve for the sand used in the concrete specimens. The sand comprises well-graded particles ranging from 0.1 to 0.8 mm, covering fine to coarse fractions to simulate a natural granular matrix and enhance packing efficiency.

Table 1 XRF analyses of cement, sand particles, and kaolinite (wt%)

Chemical composition	SiO_2	Al_2O_3	BaO	CaO	Fe_2O_3	K_2O	MgO	MnO	Na_2O	P_2O_5	SO_3	TiO_2	LOI
Cement	20.53	4.27	0.05	63.43	3.21	0.71	2.85	0.16	0.35	0.05	2.51	0.31	1.57
Sand	79.86	7.44	0.08	3.96	0.44	2.93	0.25	0.14	1.78	-	1.32	0.06	1.49
Kaolinite	59.86	19.21	-	1.54	5.28	2.26	2.53	0.07	1.16	0.12	-	1.14	6.83

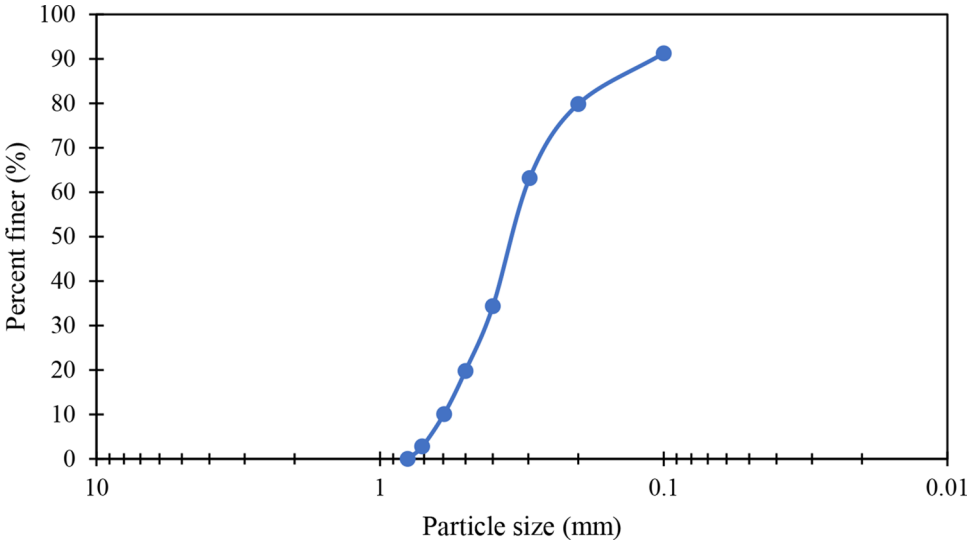

Fig. 1 Grain size distribution of samples

Table 2 Salt concentration used to prepare different conditions of the curing process

Salt solution ID	Salt	Concentration (g/L)
A	NaCl	10
B	Na_2SO_4	10
C	$CaCl_2.2H_2O$	10
D	$MgCl_2.6H_2O$	10
E	NaCl	15
F	Na_2SO_4	15
G	$CaCl_2.2H_2O$	15
H	$MgCl_2.6H_2O$	15
I	NaCl	30
J	Na_2SO_4	30
K	$CaCl_2.2H_2O$	30
L	$MgCl_2.6H_2O$	30

It is worth mentioning that the selected mass proportions of the components (i.e., 72 wt% sand, 11 wt% Portland cement, 5 wt% kaolinite clay, and 12 wt% water) were adopted from Shakiba et al. (2020a). This composition has been validated in prior studies for achieving structural integrity, realistic porosity and permeability values, and consistent mechanical properties in synthetic porous samples, making it suitable for the targeted analysis of salt interactions during curing. It should be noted that samples need to be cured to carry out physical and mechanical laboratory tests. In this regard, a series of salt solutions at three distinct concentrations were considered to provide various curing conditions, as presented in Table 2:

The selection of salts (NaCl, Na_2SO_4, $CaCl_2{\cdot}2H_2O$, and $MgCl_2{\cdot}6H_2O$) was based on their common occurrence in naturally saline environments, brines, and formation waters in regions with arid or semi-arid climates, including the Middle East. These ions are frequently encountered in geotechnical and reservoir engineering operations in Iran and similar contexts, making the experimental conditions representative of real-world engineering challenges involving salt exposure. The chosen salt concentrations (i.e., 10, 15, and 30 g/L) represent a range of salinities commonly found in saline groundwater, formation brines, and industrial wastewater, and are based on reported ranges in regional geochemical data and previous experimental studies involving ion–cement interactions [33, 35, 36].

It is noteworthy that the chemical composition of curing fluids, especially the type and concentration of dissolved salts, can significantly influence hydration kinetics, cement–ion reactions, and ultimately, the formation of the hardened matrix. Ions such as Na^+, K^+, Mg^{2+}, and SO_4^{2-} interact with hydration products like C-S-H, portlandite, and ettringite, leading to structural and chemical modifications in the cementitious framework.

Sample Preparing procedure

In the present study, the sandstone composition proposed by Shakiba et al. (2020a) was applied to prepare concrete specimens. According to the ASTM C305 procedure, the preparation involved mixing 12 wt% water, 11 wt% cement, 5 wt% clay mineral, and 72 wt% sand [32]. These constituents were blended using a mechanical mixer until a homogenous mixture was achieved. The resulting mortar was poured into cylindrical molds, and a vibrator plate was used to eliminate any trapped air or voids. The molds were then placed in an absorption oven at 25 °C and nearly 100% humidity for 24 h to enable initial curing. After demolding, specimens were immersed in saturated calcite solutions containing the selected salts for a 28-day curing period. This process facilitated pore interconnectivity and enhanced cementation [37, 38]. The calcite solution facilitates additional calcium ion availability, promoting further nucleation of calcium-rich phases (e.g., C-S-H) and enhancing the degree of cementation and inter-particle bonding. This also helps establish more continuous pore networks while enabling ion exchange with the introduced salts [39]. Upon completion of curing, the samples were dried at 100 °C to remove moisture before testing, and then trimmed for physical and mechanical evaluations. It should be noted that the drying step was conducted after full curing and was applied uniformly across all samples. This ensured consistent moisture removal while avoiding disruption of early hydration or salt crystallization processes. Figure 2 shows the samples after the initial and final curing processes.

The absorption oven used during the initial 24-hour curing stage operated at a controlled temperature of 25 °C and near-saturated humidity (~ 100%) to facilitate primary hydration without premature drying. After the final 28-day curing in salt solutions, the concrete specimens were dried at 100 °C to remove moisture prior to testing. This temperature was selected to ensure consistent comparison across all samples. Since the hydration reactions and ion–cement interactions had largely completed during the 28-day curing phase, the thermal treatment did not significantly influence the final microstructure or mechanical performance. Similar post-curing drying protocols have been applied in earlier studies [32, 40, 41]. Although 100 °C is relatively high for drying cementitious materials, the thermal treatment was performed after the completion of

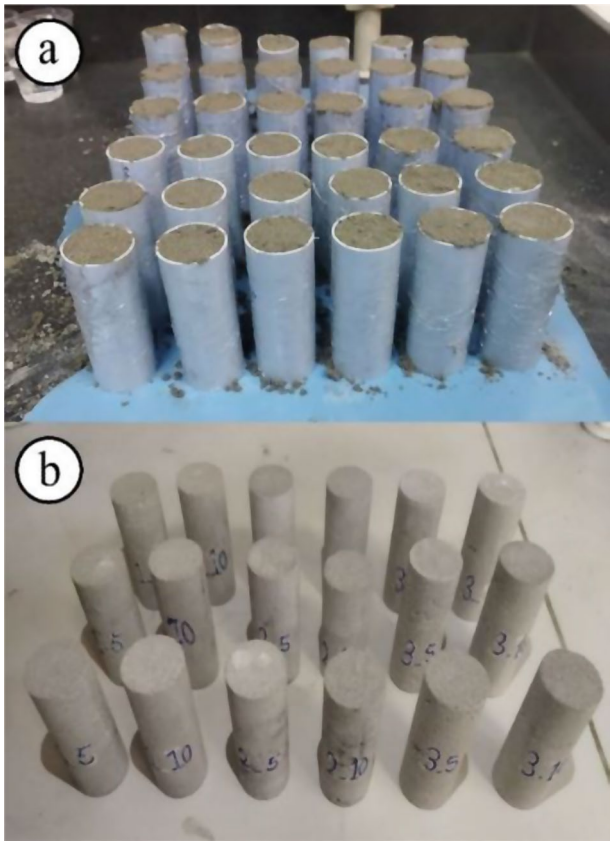

Fig. 2 Concrete samples after initial and final curing processes

the 28-day curing process when hydration and salt precipitation had stabilized. Moreover, while some degree of salt recrystallization or thermal microcracking could occur under elevated temperatures [18], this risk was minimized by the fact that the samples were fully cured beforehand. Additionally, since all specimens were subjected to the same post-curing drying conditions, any potential microstructural changes would have occurred uniformly, thereby preserving the integrity of comparative analysis across different salt treatments. It is noteworthy that each measurement was replicated three times to ensure repeatability, and reported physical and mechanical results represent average values. The physical properties of the specimens are given in Table 3.

Results

Chemical reaction products

Chemical reactions between clay minerals, cement, and salts would result in new products that may change the samples primary physical and mechanical properties. In this regard, XRD analysis can detect chemical products and even residual reactants [42]. It is worth mentioning that XRD analyses were measured in operating conditions of 60 kV, 60 mA current, 0.0310 (2θ) step size, and 10° to 70° scanning range for samples with the lowest salt concentration (1–4) and the highest ion concentration (9–12). It is noteworthy that in the present study, samples from the lowest (10 g/L) and highest (30 g/L) concentrations were selected for XRD and FTIR to highlight the contrast between minimal and extensive salt–cement interactions. These represent the chemical reactivity boundaries in the experimental design. Figures 3 and 4 illustrate XRD analyses of samples.

Table 3 Physical properties of samples

Sample	Salt solution	Length (mm)	Standard deviation (length)	Diameter (mm)	Standard deviation (diameter)	Grain density (g/cm^3)
1	A	75.11	0.15	36.35	0.05	2.559
2	B	74.57	0.06	36.30	0.07	2.554
3	C	74.57	0.13	37.00	0.13	2.565
4	D	74.56	0.07	37.22	0.05	2.562
5	E	74.77	0.04	37.35	0.06	2.564
6	F	74.39	0.07	36.82	0.08	2.557
7	G	75.09	0.03	36.25	0.05	2.564
8	H	74.58	0.11	36.97	0.09	2.567
9	I	74.60	0.06	36.47	0.06	2.567
10	J	74.74	0.05	37.20	0.06	2.558
11	K	74.36	0.06	37.05	0.06	2.563
12	L	74.53	0.07	36.83	0.07	2.572

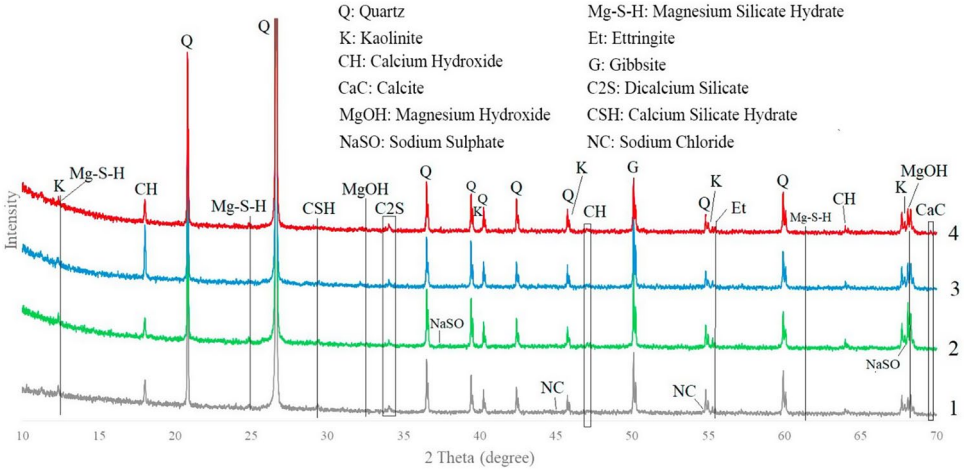

Fig. 3 XRD analyses of samples 1–4

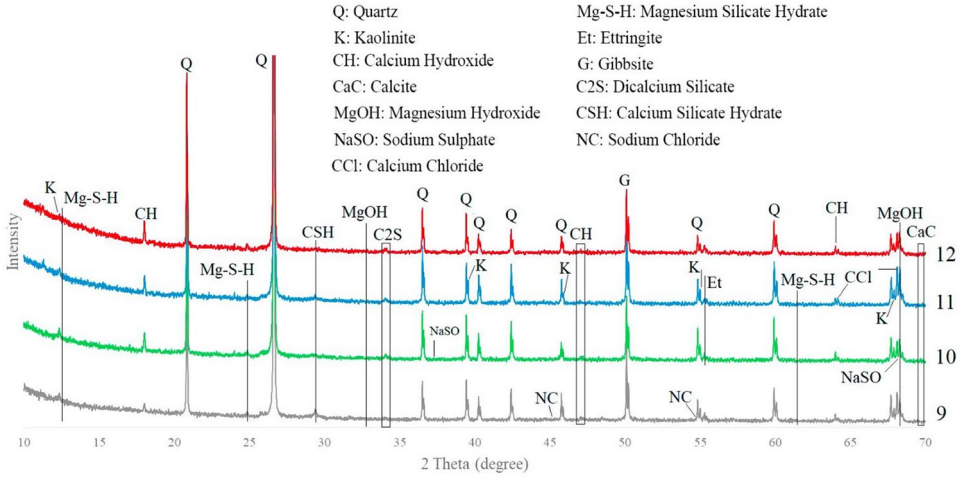

Fig. 4 XRD analyses of samples 9–12

Table 4 Chemical components resulting from chemical reactions

Component	Chemical formula	Reaction	Reference
Calcium hydroxide (portlandite)	$Ca(OH)_2$	$CaO + H_2O \rightarrow Ca(OH)_2$	[43]
Magnesium hydroxide (brucite)	$Mg(OH)_2$	$MgO + H_2O \rightarrow Mg(OH)_2$	[44]
Magnesium silicate hydrate (lizardite)	$2Mg_3Si_2O_5(OH)_4$	$3Mg_2SiO_4 + SiO_{2+}4H_2O \rightarrow 2Mg_3Si_2O_5(OH)_4$	[45]
Ettringite	$Ca_6Al_2(SO_4)_3(OH)_{12}.26H_2O$	$6Ca^{2+}+2Al(OH)_4^-+4OH^-+3SO_4^{2-}+26H_2O \rightarrow Ca_6Al_2(SO_4)_3(OH)_{12}.26H_2O$	[46]
Gibbsite	$Al(OH)_3$	$Al_2O_3 + H_2O \rightarrow Al(OH)_3$	[47]
Calcium silicate hydrate	$3CaO{\cdot}2SiO_2{\cdot}4H_2O$	$2Ca_3SiO_5 + 7H_2O \rightarrow 3CaO{\cdot}2SiO_2{\cdot}4H_2O + 3Ca(OH)_2$	[48]

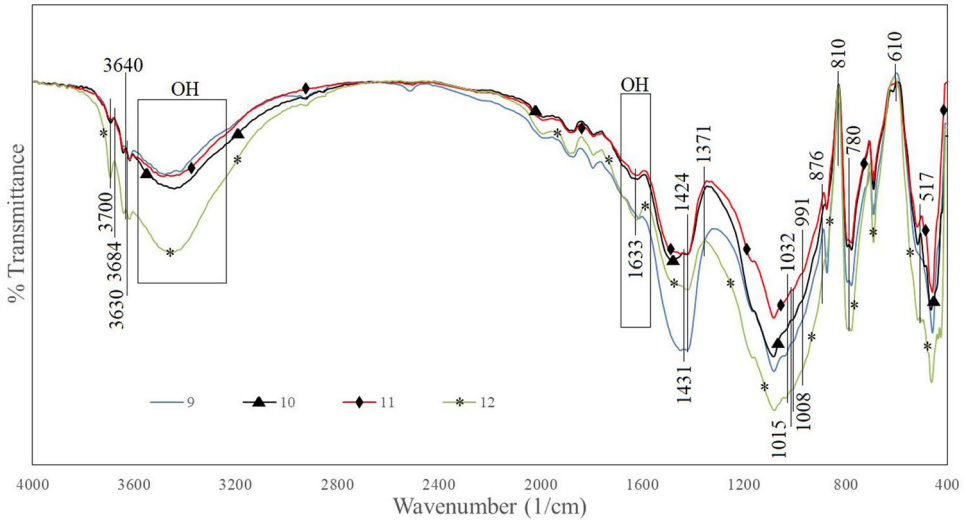

Fig. 5 FTIR spectrum of specimens 9–12

The main chemical products resulting from chemical reactions between salt/cement and concrete minerals are shown in Figs. 3 and 4 and given in Table 4. Besides, some excess reactants (i.e., salts and minerals) can be observed in XRD analyses.

Ingredients spectra of samples

The FTIR technique was performed in the 4000–400 cm^{-1} mid-infrared spectral region at 0.4 cm^{-1} resolution to collect ingredients spectra for samples 9–12. The results of XRD analyses are used in this section to strengthen FTIR outcomes. Figure 5 shows the FTIR spectrum of samples.

In this study, the FTIR analysis was applied to determine the chemical products of the reaction of cement, various salts, and kaolinite in four different fluid solutions as influential elements in forming the internal structure of samples. The FTIR test is based on the vibrations of molecular bonds of the different minerals. The position of absorption peaks in the infrared region of the electromagnetic spectrum helps to determine the molecular bonds of a mineral [49, 50]. Figure 5 illustrates the FTIR spectrum of

samples 9, 10, 11, and 12 in multiple absorption peaks concerning kaolinite (the Si–O–Si and Al–O–Si stretching peaks of the tetrahedral layer could be observed at 1032 and 1008 cm^{-1}, respectively) [51]. The peaks at 517, 780, and 810 cm^{-1} would be expected for quartz minerals, and peaks at 876 and 1424 cm^{-1} for calcium hydroxide [52]. The extensive band at 1424 cm^{-1} shows the Ca–O bond related to the carbonation of calcium hydroxide. Besides, the strong bands between 3100 and 3400 cm^{-1} can be attributed to O-H stretching and bending vibrations, and the band at about 1633 cm^{-1} corresponds to O-H vibrations, which indicates the existence of the O–H bond in calcium hydroxide [53]. Moreover, calcite has been documented to have peaks at 876 and 1431 cm^{-1} [54]. The characteristic adsorptions at 876 cm^{-1} are attributed to Si-O bending vibration (calcium silicate hydrate (CSH)) [55, 56]. In concentrated $CaCl_2$, CSH expands less than in salt solutions containing NaCl, which may likely have high-charge exchange cations firmly attracting the dipoles of water molecules surrounding them, causing a phenomenon known as dielectric saturation [57]. This phenomenon reduces the effective dielectric constant of water near the cations, limiting the mobility of water dipoles and thus suppressing hydration reactions and delaying the formation of gel-like phases such as C-S-H. Consequently, precipitation is reduced due to limited ion mobility and restricted nucleation sites [57]. In addition, an increase in the concentration of Cl^- could decrease the peak value of C-S-H because of forming $3CaO{\cdot}Al_2O_3{\cdot}3CaCl_3{\cdot}32H_2O$ as a result of the reaction between Cl^- and $3CaO{\cdot}Al_2O_3$ (C_3A) [58]. As can be seen in Figs. 3 and 4, in samples containing Mg^{2+}, the peak of CSH would decline owing to lower solubility of $Mg(OH)_2$ than $Ca(OH)_2$ [58]. The hydroxyl groups of the CSH-phases and water molecules cause a broad band in the 3100–3500 cm^{-1} region together with an -OH bending mode between 1633 and 1663 cm^{-1} [59]. The additional band can be marked in the FTIR spectra of hydrated tricalcium silicate (C_3S) at 1371 and 3640 cm^{-1} [60]. Furthermore, the dicalcium silicate (C2S) vibration would develop at around 876 cm^{-1} [61]. The FTIR spectra for $Mg(OH)_2$ (Brucite) show the absorption bands in 1015 and 3700 cm^{-1} [62, 63]. The following three bands at 610, 991, and 3684 cm^{-1} are related to vibrations of $2Mg_3Si_2O_5(OH)_4$ (Lizardite) [64, 65]. The FTIR spectra of $Ca_6Al_2(SO_4)_3(OH)_{12}.26H_2O$ (Ettringite) is located in 3630 cm^{-1} [66–68]. The presence of SO_4^{2-} in the solution (samples 2 and 10) could produce more Ettringite [58]. All the elements that emerged in FTIR and XRD analyses demonstrated that the presence of various salts and clay minerals (kaolinite in this study) in the concrete composition could produce new components presented in Table 4. It is worth mentioning that such components would influence the characteristics of the concrete. In addition, as can be seen from Figs. 3 and 4, such reactants in the porous media may also remain unreacted, and consequently, they can further affect the properties of the concrete. Over extended periods, these unreacted salts and minerals can act as latent sources of chemical reactivity, particularly under environmental fluctuations such as wetting–drying or thermal cycles. Their gradual dissolution or delayed recrystallization may initiate microcracking, promote secondary expansion, or reduce the chemical stability of the matrix, ultimately compromising long-term durability of the cementitious material. Such behavior is especially critical in saline environments where ion exchange and moisture ingress are likely to persist [69].

Key chemical bond changes observed in FTIR due to salt interactions are as follows:

- The shift in peaks of O–H and Si–O–Si, suggests altered hydration states.

- Reduced C–S–H peak intensity in Mg-rich samples indicates suppressed gel formation.
- Enhanced peaks at 1424 cm^{-1} and 876 cm^{-1} in SO_4^{2-} systems suggest ettringite and calcite precipitation.

Discussion

Salt concentration and precipitation

In this study, 12 various salt solutions have been used to prepare the aqueous phase. Total salinity and concentration of reactive ions are two main factors forming precipitation in an aqueous solution [70]. In this regard, ion activity has a remarkable effect on an indicator known as saturation index (SI), a function of the type and concentration of ions. It represents the amount of salt precipitation in a solution as Eq. 1 [33].

$$SI = \log\left(\gamma_i m_i\right)/K_{sp} \tag{1}$$

Where γ_i is the activity coefficient, m_i represents ion concentration, and K_{sp} is the solubility product. SI is a thermodynamic indicator of salt precipitation potential; positive SI values suggest oversaturation and imminent deposition of salts in pore space. Generally, negative SI values decrease precipitation, while positive quantities show an increment of deposition [70]. It should be noted that the numerator in Eq. 1 is known as ion activity. Calcite in an aqueous solution can react as Eq. 2:

$$CaCO_3 + H_2O \rightarrow Ca^{2+} + CO_3^{2-} + H^+ + (OH)^- \tag{2}$$

Calcium ions resulting from $CaCO_3$ can react with other ions (e.g., Cl^- and SO_4^{2-}) in the solution because of its high activity. Figure 6 shows the chemical reactions between salt ions and Ca^{2+} in the aqueous solution.

The main adverse products of the reaction between NaCl/Na_2SO_4 and calcite are $CaCl_2$ and $CaSO_4$. Such calcium salts comprising divalent ions can result in precipitation for even a low concentration and, thus, affect concrete physical and mechanical characteristics [71]. The reactions illustrated in Fig. 6 demonstrate how calcium carbonate in the matrix interacts with salt ions such as Cl^- and SO_4^{2-} to form calcium-based precipitates like $CaCl_2$ and $CaSO_4$. These reaction products can accumulate within the pore space, leading to physical pore-filling and thereby reducing the connectivity of flow paths. In particular, the formation of $CaSO_4$ may also contribute to expansive crystallization pressure, especially in confined pores, which can initiate microcracks and lead to mechanical degradation over time. Therefore, the reaction pathways not only alter the porosity and permeability but also play a critical role in potential strength loss under certain chemical environments.

To quantify the amount of salt precipitation in this study, the residual curing solutions from each sample container were collected at the end of the 28-day period. These solutions were filtered through 0.45 μm membrane filters to separate solid precipitates. The filtered solids were then dried at 60 °C for 24 h and weighed using a high-precision analytical balance with ± 0.001 g accuracy. The recorded mass represented the amount of salt precipitated due to chemical interactions during curing under each condition. Figure 7 illustrates the amount of salt precipitation for all solutions.

As can be seen from Fig. 7, in NaCl and Na_2SO_4, as salt concentration increased, the amount of salt precipitation increased. That is, an increase in ionic concentration can

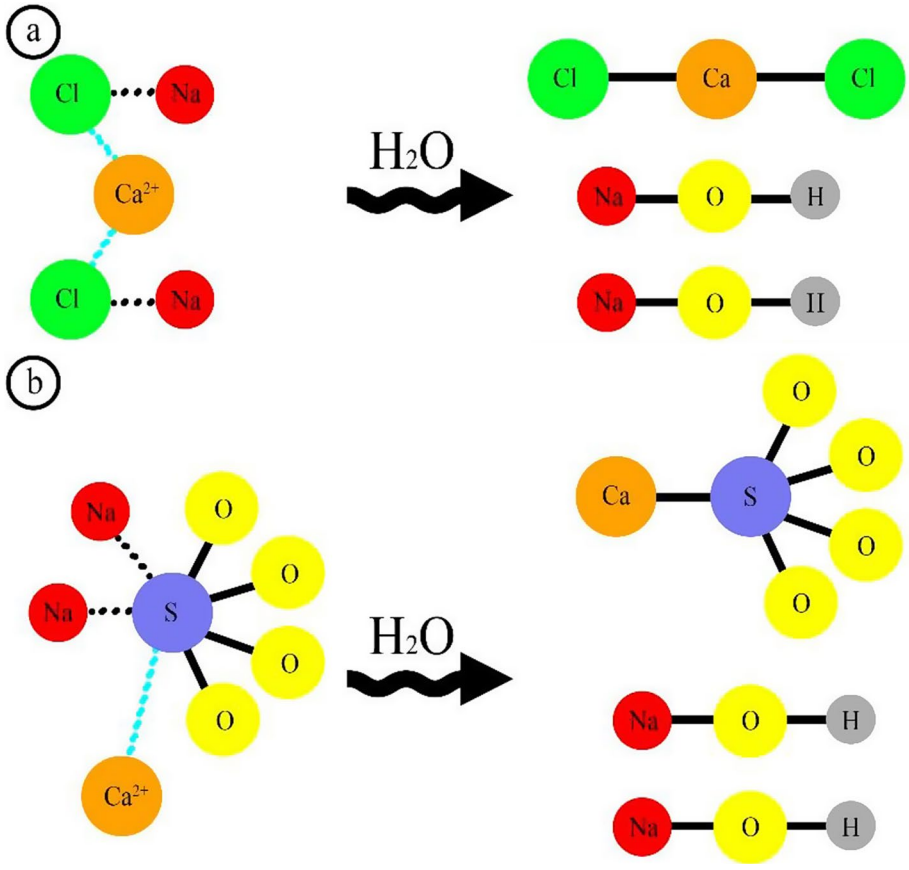

Fig. 6 (**a**) Reaction between NaCl and Ca^{2+}, (**b**) reaction between Na_2SO_4 and Ca^{2+}

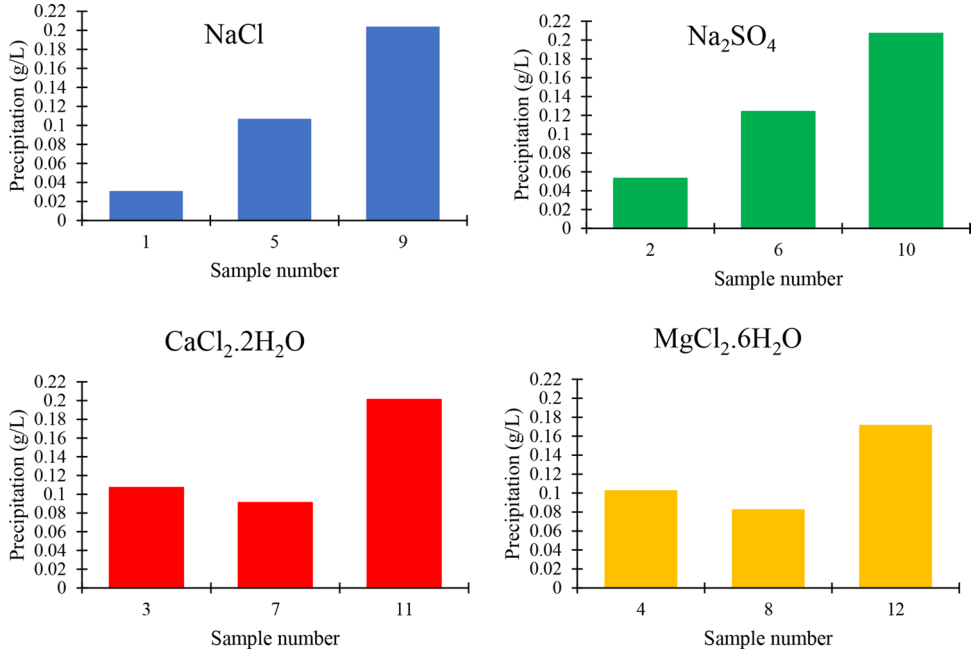

Fig. 7 Amount of salt precipitation resulting from chemical interaction between ions

lead to significant differences in the characteristics of a salty solution and influence the deposition pattern of salts [72]. Besides, based on Eq. 1, an increase in ion concentration can result in a higher SI, hence, more precipitation in the medium. The results indicated that sulfate ions could increase the total amount of precipitation. This is due to the formation of ettringite ($Ca_6Al_2(SO_4)_3(OH)_{12}{\cdot}26\ H_2O$), which is a crystalline and expansive hydration product resulting from reactions between sulfate ions and calcium/aluminum phases present in the cement matrix. Ettringite has a relatively large molar volume and tends to nucleate rapidly in sulfate-rich environments, thereby contributing significantly to solid-phase precipitation and pore filling [66, 73]. However, a synclinal trend was observed for salt solutions comprising divalent cations (i.e., Ca^{2+} and Mg^{2+}). Various transport processes such as capillary flow and diffusion mechanisms, often result in disruptive expansion due to detrimental reactions between diverse ions and the hydrated cement phase in the pore space [69]. Hence, the presence of calcium and magnesium ions in the solution could form ettringite and lizardite as prone elements to precipitate [73, 74]. For salt concentration higher than 15 g/L (i.e., solutions 11 and 12), more concentration of a reactive ion in solution (i.e., Ca^{2+} or Mg^{2+}) could lead to an increase in both ion activity and solubility product and, therefore, more precipitation in the medium would be [33]. For salt concentrations lower than 15 g/L (i.e., samples 3 and 4), although salt concentration decreased, the activity of Ca^{2+} as the reactive ion would prevail over the salinity. Consequently, total salt precipitation would increase as well. That is, under such conditions, the activity of the reactive ion could play a pivotal role in intensifying total precipitation [33, 71]. According to the results, the concentration of 15 g/L of $CaCl_2.2H_2O$ and $MgCl_2.6H_2O$ should be considered an optimum point for the least salt precipitation. This optimum concentration has practical implications in engineering design, particularly for the formulation of cementitious systems used in saline aquifers, oil and gas wells, or groundwater control structures. Maintaining salt concentrations near this threshold may help minimize detrimental precipitation, preserve permeability, and enhance long-term durability without compromising early-age strength. For instance, in reservoir cementing or underground grouting, brine chemistry can be adjusted to target such optimal salinity levels, thereby mitigating formation damage while maintaining structural integrity [33, 71]. It should be noted that magnesium ion has a moderate influence on the enhancement of salt precipitation compared to calcium ion owing to its lower chemical activity than that of calcium [75]. Sulfate ions can neutralize the decreasing effect of magnesium on precipitation [33]. Therefore, if no sulfate ions were in the solution, the role of magnesium ions in the reduction of total salt deposition would be more sensible, especially for high precipitations, as for the same concentration of calcium and magnesium of 30 g/L, magnesium brine resulted in 15% lower precipitation. A series of magnified FESEM images taken from thin slabs of specimens also show the detrimental influence of precipitation on pore surfaces, resulting in changing primary physical characteristics of the concrete, as illustrated in Fig. 8.

In Fig. 8a and f, the borders between interconnected pore throats and salt precipitations were highlighted in red. As observed in the FESEM images, samples cured in lower salt concentrations (i.e., Fig. 8a, d and g, and 8j) retain relatively clean and open pore surfaces, with fewer crystal formations. In contrast, samples treated with higher salt concentrations (i.e., Fig. 8c, f and i, and 8l) exhibit dense accumulations of crystalline precipitates along pore walls and throats. These precipitates often appear as angular

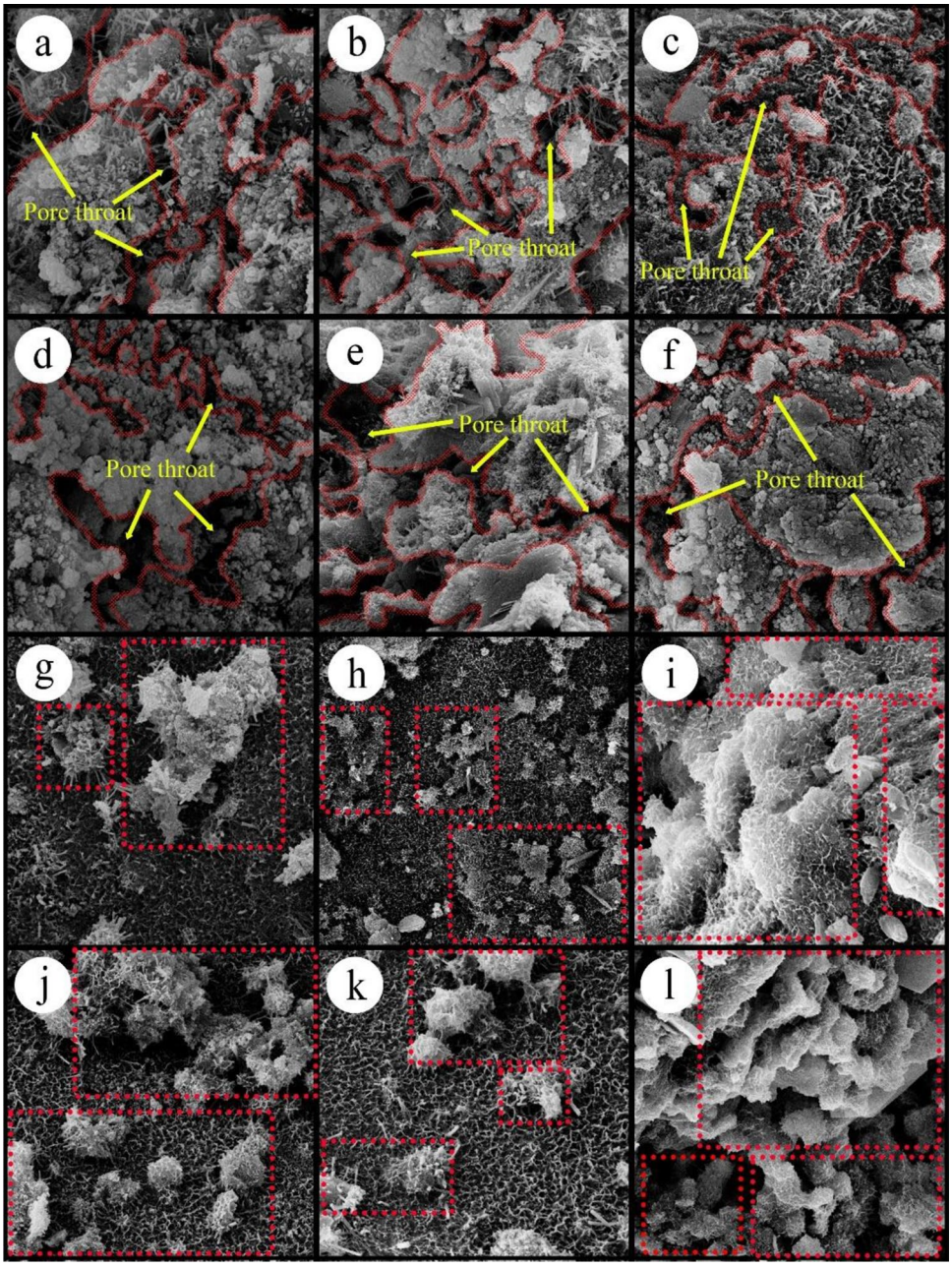

Fig. 8 FESEM images of samples including (**a**) NaCl 10 g/L, (**b**) NaCl 15 g/L, (**c**) NaCl 30 g/L, (**d**) Na_2SO_4 10 g/L, (**e**) Na_2SO_4 15 g/L, (**f**) Na_2SO_4 30 g/L, (**g**) $CaCl_2.2H_2O$ 10 g/L, (**h**) $CaCl_2.2H_2O$ 15 g/L, (**i**) $CaCl_2.2H_2O$ 30 g/L, (**j**) $MgCl_2.6H_2O$ 10 g/L, (**k**) $MgCl_2.6H_2O$ 15 g/L, (**l**) $MgCl_2.6H_2O$ 30 g/L (view field: 26.22 µm). Red dotted lines in subfigures (**g**) to (**l**) highlight visible accumulations of salt crystals within pore regions, based on morphology and contrast. Although no EDS analysis was conducted, the precipitation zones correspond to known salt types used in each curing condition

or needle-like structures that partially or fully obstruct interconnected pore channels. Particularly in samples with divalent cations at 15 g/L (Fig. 8h and k), the microstructure appears more stable with minimal pore clogging. These observations provide visual confirmation of the correlation between salt concentration and pore accessibility, reinforcing the permeability and porosity trends described earlier [22, 38, 74].

According to Fig. 8, in samples comprising NaCl and Na_2SO_4, as salt concentration increased, the concrete surface would be influenced by chemical interactions. Moreover, as can be observed in Fig. 8h and k, the lowest chemical precipitation associated with divalent cations would be formed at 15 g/L concentrations for both $CaCl_2.2H_2O$ and $MgCl_2.6H_2O$ salts.

Physical and mechanical properties

Generally, two mechanisms can be identified for salt transport by water in a porous material. The first is diffusion, which tends to even out accumulations but is relatively slow in porous materials. Capillary flow is considered the second mechanism, which is most efficient and typically faster than diffusion. Water can transport salts when liquid, while they can be retained in the vapor phase. The capillarity mechanism controls liquid water, while the diffusion mechanism controls water vapor. In more detail, capillary flow occurs when liquid water is drawn through narrow interconnected pores due to surface tension forces and pressure gradients. This mechanism dominates during the early stages of drying or in fully saturated systems and results in relatively fast and directional movement of dissolved salts. As water evaporates at the surface, also known as the drying front, salts are transported via liquid films toward these regions and subsequently precipitate, typically forming crusts or visible salt deposits called efflorescence. On the other hand, diffusion governs salt transport in the vapor phase, particularly under lower humidity conditions or in partially saturated pore structures. Driven by concentration gradients, this process is slower and leads to a more gradual and spatially distributed movement of salts throughout the pore network. In drying cementitious materials, both mechanisms may operate simultaneously. Capillary flow tends to concentrate salts at exposed surfaces, while diffusion enables redistribution within the interior. The dynamic balance between these two mechanisms significantly affects the location and morphology of salt precipitation, which in turn impacts pore blockage, permeability, and long-term durability of the material [76, 77]. Figure 9 schematically depicts these mechanisms.

These two mechanisms would inevitably compete in the porous material [76]. Thus, any precipitation in the porous media could be an obstacle that affects fluid flow, and as

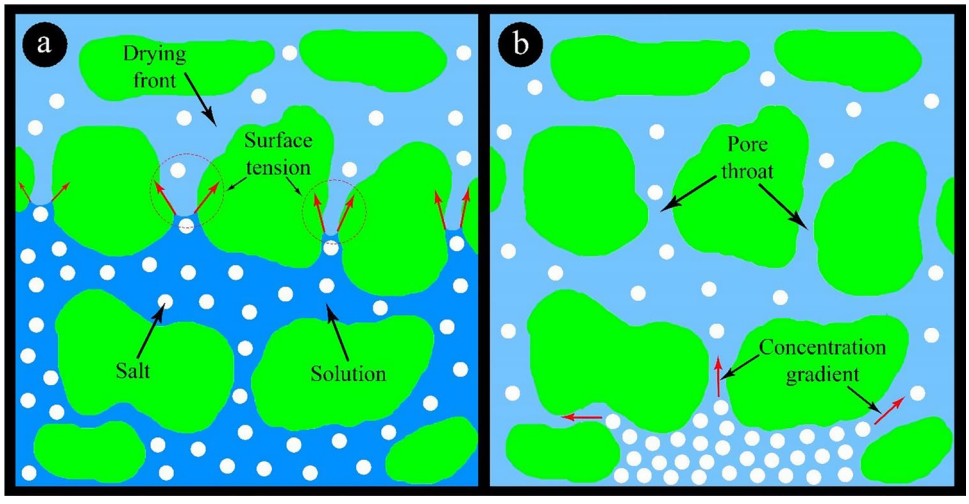

Fig. 9 Conceptual illustration of salt transport mechanisms: (**a**) capillary flow driven by surface tension and pore connectivity enables rapid salt migration and accumulation at drying fronts; (**b**) diffusion dominates vapor-phase transport, leading to gradual redistribution of dissolved salts across the pore space

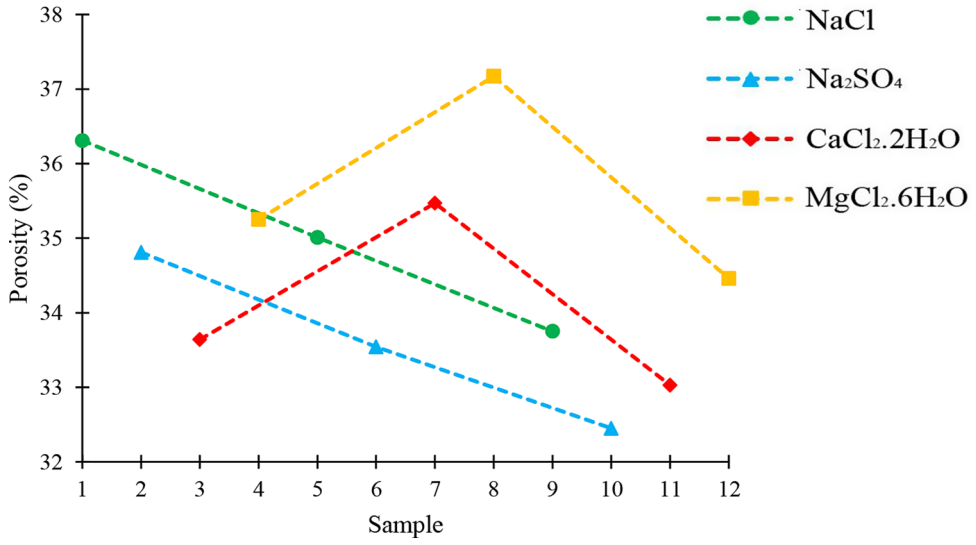

Fig. 10 The impacts of type and concentration of various salts on the porosity of the specimens

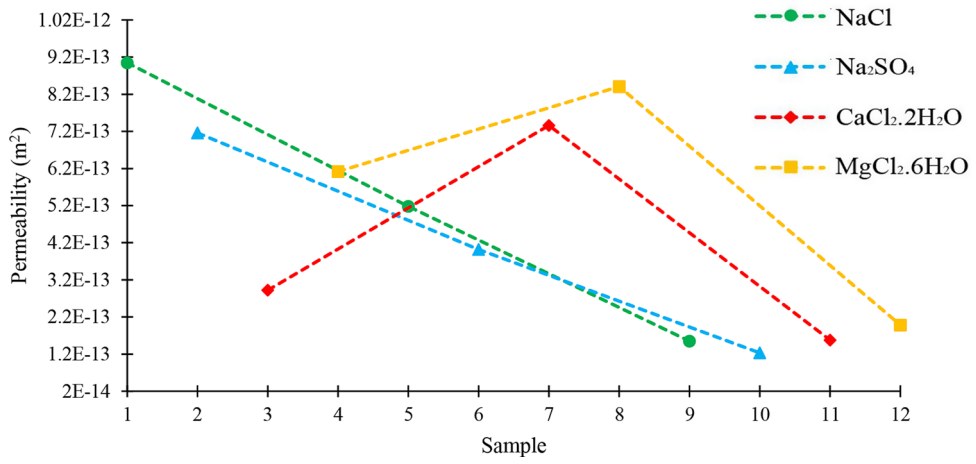

Fig. 11 The effects of type and concentration of various salts on permeability of the specimens

a result, it would alter rock properties such as porosity, permeability, and rock strength [22, 78–80]. Due to capillary flow, salt concentrations in the liquid phase are highest at the surface of pores, leading to preferential precipitation at the surface, so-called efflorescence phenomenon [20]. During precipitation, permeability decreases due to a reduction in porosity. Nevertheless, permeability can alter by several orders of magnitude for diverse dissolution/precipitation processes under varying reactive transport conditions, regardless of whether the porosity remains the same or not [77]. Figures 10 and 11 show concrete porosity and permeability for all samples, respectively.

Figures 10 and 11 indicate that concrete porosity and permeability were indirectly related to the total precipitation amount. At the same time, their relationship with salt concentration depended on ion types in salt (i.e., monovalent or divalent ions). Samples containing NaCl and Na_2SO_4 showed a decreasing trend associated with salt precipitation. Nevertheless, changes in the concentration of divalent cations (i.e., Ca^{2+} and Mg^{2+}) demonstrated an anticlinal mode on the primary physical properties of concrete, resulting from findings in Fig. 7. In this regard, concrete permeability is much more

susceptible to changes in salt precipitation than concrete porosity due to pore throat blockage. In other words, unlike total porosity, permeability is governed by interconnected pore throats, which are more susceptible to blockage by localized crystal growth [37, 38]. Bacci et al. (2011) also reported such an observation when they injected CO_2 into saline aquifers [17]. For instance, a 50% change in calcium chloride content could alter concrete porosity and permeability by about 5% and 60%, respectively. This indicates that salt precipitation in porous media can severely affect flow paths compared to total void volume. Such a feature would be significant in porous materials, where fluid flow is much more important than storage capacity. Furthermore, a series of samples were tested, and the results indicated inverse relationships between concrete porosity and compressional and shear sonic wave velocities, as shown in Fig. 12.

The correlations between porosity–sonic velocities may serve as a basis for nondestructive evaluation of concrete curing and internal degradation under saline conditions. Based on Fig. 12, both linear and exponential relationships demonstrate good data matching as their squared regression coefficient values considerably approach one, and thus, they can be used to predict the relation between concrete porosity and sonic wave velocity. A comparative evaluation of the linear and exponential fits for the relationship between porosity and sonic wave velocity was performed using the coefficient of determination (R^2). The exponential fits achieved R^2 value of 0.96 and 0.97, indicating a very strong correlation, while the linear fit resulted in a slightly lower R^2 of 0.96. Given the improved accuracy and better data representation, the exponential model was selected as the preferred fit to describe the dependence of sonic wave velocity on porosity in the concrete samples. It should be noted that structurally analogous specimens would reduce pore geometry effects on such relationships [81]. Increasing salt precipitation can impact concrete porosity by blocking interconnected pores. As a result, concrete structural integrity and internal continuity would improve. The same composition and preparation process of porous concrete samples could compensate for the impacts of some adverse factors, such as type of porosity and pore geometry, on the relationship between concrete porosity and sonic wave velocity. However, comparing current data and our previous outcomes reveals that distinct salts in initial water composition could increase compressional sonic wave velocity up to about 16% [82]. To investigate the impact of salt precipitation on concrete porosity and strength, a series of uniaxial

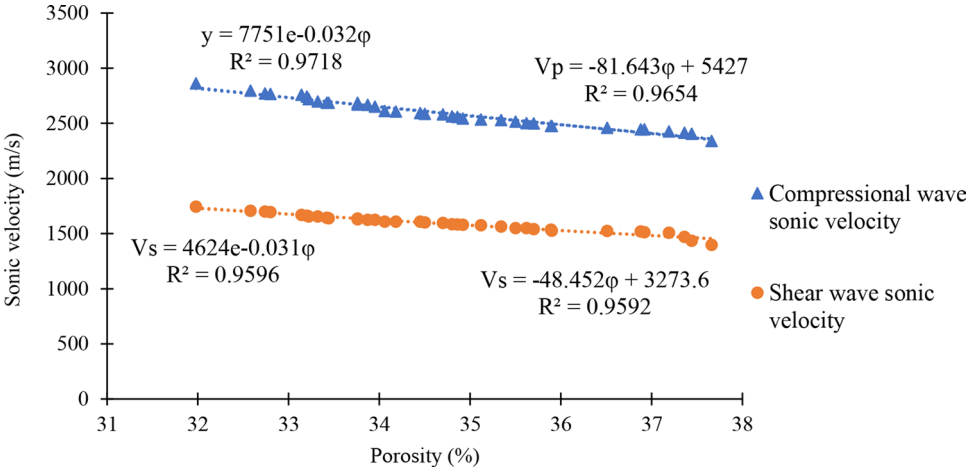

Fig. 12 The relationship between concrete porosity and sonic wave velocity

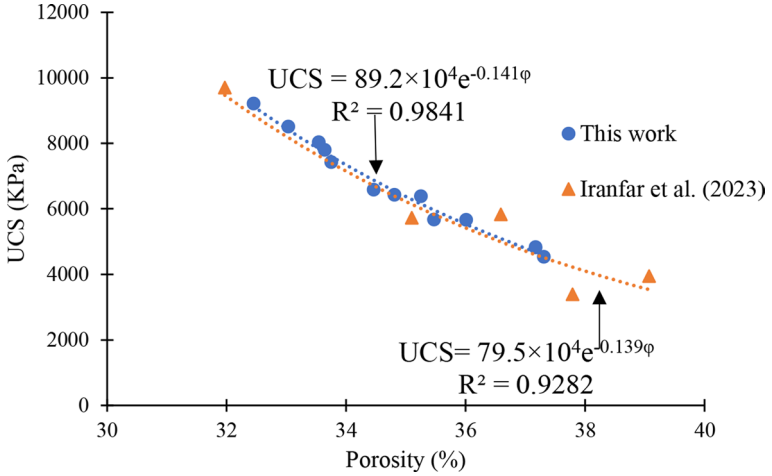

Fig. 13 UCS data in terms of concrete porosity of the current study and data from Iranfar et al. (2023) [82]

compressive strength (UCS) tests were performed on specimens. Moreover, for benchmarking purposes, UCS–porosity data from Iranfar et al. (2023) was used in comparison with the present results, as both studies employed artificial porous concrete specimens with identical cement content (11 wt%) and similar mix design and curing protocols [82]. This consistency supports a valid comparison of mechanical behavior trends. The results are presented in Fig. 13:

Porosity as a discontinuity in concrete structure could lessen the strength of a concrete under compressive and tensile stresses. Figure 13 illustrates an inverse exponential relationship between concrete porosity and UCS, which agrees with our previous study on artificial samples with the same cement content [82]. While porosity is a major control on UCS, the presence of dissolved salts may also influence mechanical strength independently through chemical means. Specifically, certain salts promote the formation of additional crystalline phases (e.g., ettringite, brucite, or modified C-S-H), which can enhance particle bonding or matrix densification. Conversely, excessive salt content or aggressive ion interactions may introduce microcracking or heterogeneous precipitation zones that locally weaken the structure. Therefore, the impact of salts on UCS reflects a combination of physical pore alteration and chemical reinforcement or degradation depending on the salt type and concentration [54, 67, 81]. The results also showed that various salts in an aqueous solution could increase the accuracy of the exponential correlation between the UCS and porosity of the concrete. It has been established that heterogeneous pore size distributions on the surface of pores cause preferential efflorescence occurring exclusively at fine pores [11]. The exponential relationship observed between UCS and porosity provides a practical tool for predicting strength behavior in salt-affected cementitious materials. In field applications, porosity can be measured more readily than strength, particularly using non-destructive techniques such as sonic or imaging-based methods. This relationship can therefore serve as a design criterion for selecting appropriate curing strategies or material formulations in environments where salt exposure is likely, ensuring sufficient strength development while accounting for microstructural changes induced by salt precipitation. Given that the structural characteristics of artificial porous samples can be controlled, they can be widely used to study the effect of each influential factor on primary mechanical and physical properties.

Conclusions

The principal objective of this study was to evaluate how the type and concentration of dissolved salts influence precipitation behavior and its effect on the primary physical and mechanical properties of porous cementitious materials during curing. The key findings can be summarized as follows:

- The results indicated that concrete permeability is significantly more sensitive to salt concentration than porosity. For example, a 50% increase in salt concentration reduced porosity by only 5%, whereas it caused a 60% decrease in permeability, highlighting the vulnerability of flow paths to pore throat blockage.
- The concentration of monovalent ions was inversely proportional to the porosity and permeability of concrete due to the ion activity relating to SI factor. For divalent ions (i.e., Ca^{2+}, Mg^{2+}), an optimum salt concentration of 15 g/L was identified, at which the minimum precipitation occurred, leading to the highest measured porosity and permeability values. This insight is particularly valuable for designing salt-tolerant cementitious materials in environments prone to chemical interaction with brine, where exceeding this threshold could result in increased pore blockage and strength loss. For instance, in samples containing magnesium chloride, salt concentrations lower (10 g/L) and upper (30 g/L) than the optimum point would enhance the precipitation up to 24% and 107%, respectively. These quantities for a calcium chloride sample were 18% and 121%, respectively.
- Residual reactants from salt–cement–clay interactions modified the internal structure of the concrete, increasing compressional wave velocity by up to 16%. This increase is associated with enhanced bonding, matrix densification, and improved continuity, indicating better material quality and durability in saline environments, and also helped define a reliable exponential relationship between UCS and porosity.

These findings offer practical values for material selection and design in geotechnical, structural, and subsurface engineering projects where salt exposure during curing is likely, such as in saline aquifers, coastal zones, or arid climates with saline groundwater. By identifying optimal salt concentrations that minimize precipitation and preserve porosity and permeability, this study supports the development of more durable cementitious systems under chemically aggressive conditions. However, it should be noted that the study was conducted using artificial samples with fixed composition and a controlled curing period of 28 days. Moreover, the environmental conditions were static and did not include thermal or moisture fluctuations often encountered in the field. Future research should focus on validating these outcomes under more realistic and dynamic environmental scenarios.

These findings are practically applicable to the formulation and curing of cementitious materials in environments exposed to saline water, such as coastal infrastructure, underground formations, and oil and gas wells. The correlation between porosity and mechanical/sonic properties also offers a basis for non-destructive monitoring during curing. Nevertheless, the study was conducted under controlled laboratory conditions using synthetic specimens and fixed curing time. Future research should assess the long-term durability of similar systems under cyclic wetting–drying, thermal, and chemical conditions, and various mechanical loads to capture real-world variability.

Abbreviations

PSD	Pore Size Distribution
SEM	Scanning Electron Microscopy
XRF	X-ray Fluorescence spectrometry
LOI	Loss on Ignition
XRD	X-ray Diffraction
FTIR	Fourier-Transform Infrared Spectroscopy
C-S-H	Calcium Silicate Hydrate
C_3S	Tricalcium Silicate
C_2S	Dicalcium Silicate
SI	Saturation Index
FESEM	Field Emission Scanning Electron Microscopy
UCS	Uniaxial Compressive Strength

Author contributions
M.M.K.: Writing the main manuscript, Data curation, Formal analysis. S.I. Writing the main manuscript, Data curation, Formal analysis. M.H.S.: Visualization, Writing the main manuscript, Writing-review and editing the main manuscript. M.S.: Conceptualization, Methodology, Visualization, Writing-review and editing the main manuscript, Supervision.

Funding
The authors did not receive support from any organization for the submitted work.

Data availability
Data sets used during the current study are available from the corresponding author on reasonable request.

Declarations

Competing interests
The authors declare no competing interests.

Received: 12 March 2025 / Accepted: 14 August 2025
Published online: 29 August 2025

References

1. Mahmoud M, Elkatatny S, Abdelgawad KZ (2017) Using high- and low-salinity seawater injection to maintain the oil reservoir pressure without damage. J Pet Explor Prod Technol 7:589–596. https://doi.org/10.1007/s13202-016-0279-x
2. Villardi HGD, Yokoyama L, Young A, Veiga AA, Pagnin S (2022) Experimental methodology for CO2 capture and sodium bicarbonate synthesis with producedwater from oil industry. J Pet Explor Prod Technol 12:2577–2585. https://doi.org/10.1007/s13202-022-01479-0
3. Taheri-Shakib J, Naderi H, Salimidelshad Y, Teymouri A, Shekarifard A (2018) Using ultrasonic as a new approach for elimination of inorganic scales (NaCl): an experimental study. J Pet Explor Prod Technol 8:553–564. https://doi.org/10.1007/s13202-017-0369-4
4. Rad MN, Shokri N, Keshmiri A, Withers PJ (2015) Effects of grain and pore size on salt precipitation during evaporation from porous media, transp. Porous Media 110:281–294. https://doi.org/10.1007/s11242-015-0515-8
5. Miri R, Hellevang H (2016) Salt precipitation during CO2 storage-A review. Int J Greenh Gas Control 51:136–147. https://doi.org/10.1016/j.ijggc.2016.05.015
6. Li X, Shi F (2021) Effects of evolving salt precipitation on the evaporation and temperature of sandy soil with a fixed groundwater table. Vadose Zo J 20:1–12. https://doi.org/10.1002/vzj2.20122
7. de Carteret R, Buzzi O, Fityus S, Liu X (2014) Effect of naturally occurring salts on tensile and shear strength of sealed granular road pavements. J Mater Civ Eng 26. https://doi.org/10.1061/(asce)mt.1943-5533.0000938
8. Akindipe D, Saraji S, Piri M (2021) Salt precipitation during geological sequestration of supercritical CO2 in saline aquifers: A pore-scale experimental investigation. Adv Water Resour 155:104011
9. Dashtian H, Wang H, Sahimi M (2017) Nucleation of salt crystals in clay minerals: molecular dynamics simulation. J Phys Chem Lett 8:3166–3172
10. Dashtian H, Shokri N, Sahimi M (2018) Pore-network model of evaporation-induced salt precipitation in porous media: the effect of correlations and heterogeneity. Adv Water Resour 112:59–71
11. Rad MN, Shokri N, Sahimi M (2013) Pore-scale dynamics of salt precipitation in drying porous media. Phys Rev E 88:32404
12. Zehnder K, Arnold A (1989) Crystal growth in salt efflorescence. J Cryst Growth 97:513–521
13. Pruess K, Müller N (2009) Formation dry-out from CO2 injection into saline aquifers: 1. Effects of solids precipitation and their mitigation. Water Resour Res 45(3). https://doi.org/10.1029/2008WR007101
14. Muller N, Qi R, Mackie E, Pruess K, Blunt MJ (2009) CO2 injection impairment due to halite precipitation. Energy Procedia 1:3507–3514
15. Yu S, Oguchi CT (2009) Complex relationships between salt type and rock properties in a durability experiment of multiple salt–rock treatments. Earth Surf Process Land 34:2096–2110
16. Shahidzadeh-Bonn N, Desarnaud J, Bertrand F, Chateau X, Bonn D (2010) Damage in porous media due to salt crystallization. Phys Rev E 81:66110
17. Bacci G, Korre A, Durucan S (2011) Experimental investigation into salt precipitation during CO2 injection in saline aquifers. Energy Procedia 4:4450–4456
18. Espinosa-Marzal RM, Scherer GW (2013) Impact of in-pore salt crystallization on transport properties. Environ Earth Sci 69:2657–2669

19. Tang Y, Yang R, Du Z, Zeng F (2015) Experimental study of formation damage caused by complete water vaporization and salt precipitation in sandstone reservoirs, transp. Porous Media 107:205–218
20. Shokri-Kuehni SMS, Vetter T, Webb C, Shokri N (2017) New insights into saline water evaporation from porous media: complex interaction between evaporation rates, precipitation, and surface temperature. Geophys Res Lett 44:5504–5510
21. He D, Jiang P, Xu R (2019) Pore-scale experimental investigation of the effect of supercritical CO2 injection rate and surface wettability on salt precipitation. Environ Sci Technol 53:14744–14751
22. Zhang D, Kang Y, Selvadurai APS, You L (2020) Experimental investigation of the effect of salt precipitation on the physical and mechanical properties of a tight sandstone, rock mech. Rock Eng 53:4367–4380
23. Zhang Y, Ju B, Zhang M, Wang C, Zeng F, Hu R, Yang L (2022) The effect of salt precipitation on the petrophysical properties and the adsorption capacity of shale matrix based on the porous structure reconstruction. Fuel 310:122287
24. Yang S-Q, Xu S-B, Liu Z, Sun B-W, Yin P-F (2023) Experimental investigation on the triaxial unloading mechanical characteristics of sandstone immersed in different brines, geomech. Geophys. Geo-Energy Geo-Resources 9:71
25. Almutairi A, Wang Y, Le-Hussain F (2023) Effect of type of ion and temperature on fines migration induced by mineral reactions during water injection into carbonate rocks. J Environ Manage 342:118193
26. Zeng L, Dautriat J, Monmusson L, Xie Q (2023) Effect of fluid saturation and salinity on sandstone rock weakening: experimental investigations and interpretations from physicochemical perspective. Acta Geotech 18:171–186
27. Hosseini E, Nazar DM, Hosseini N, Sarmadivaleh M (2024) Developing a phenomenological model to simulate single and mixed scale formation during flow in porous media: coupling a salt precipitation model with an ion transport equation under dynamic conditions. Pet Res 9:17–36
28. Bernabé Y, Fryer DT, Hayes JA (1992) The effect of cement on the strength of granular rocks. Geophys Res Lett 19:1511–1514
29. Nouri A, Vaziri H, Kuru E (2006) Numerical investigation of sand production under realistic reservoir/well flow conditions. Can Int Pet Conf 2006 CIPC 2006. https://doi.org/10.2118/2006-093
30. Singh KK, Singh DN, Ranjith PG (2014) Simulating flow through fractures in a rock mass using analog material. Int J Geomech 14:8–19. https://doi.org/10.1061/(asce)gm.1943-5622.0000295
31. Falcon-Suarez IH, Amalokwu K, Delgado-Martin J, Callow B, Robert K, North L, Sahoo SK, Best AI (2019) Comparison of stress-dependent geophysical, hydraulic and mechanical properties of synthetic and natural sandstones for reservoir characterization and monitoring studies. Geophys Prospect 67:784–803
32. Shakiba M, Khamehchi E, Fahimifar A, Dabir B (2020) An experimental investigation of the proportion of mortar components on physical and Geomechanical characteristics of unconsolidated artificial reservoir sandstones. J Pet Sci Eng 189:107022. https://doi.org/10.1016/j.petrol.2020.107022
33. Shakiba M, Khamehchi E, Fahimifar A, Dabir B (2020) A mechanistic study of smart water injection in the presence of nanoparticles for sand production control in unconsolidated sandstone reservoirs. J Mol Liq 319:114210. https://doi.org/10.1016/j.molliq.2020.114210
34. Kulanthaivel P, Soundara B, Das A (2020) Performance study on stabilization of fine grained clay soils using calcium source producing microbes. KSCE J Civ Eng 24:2631–2642. https://doi.org/10.1007/s12205-020-2028-4
35. Fidelibus MD, Balacco G, Alfio MR, Arfaoui M, Bassukas D, Güler C, Hamzaoui-azaza F, Külls C, Panagopoulos A, Parisi A, Sachsamanoglou E (2025) A chloride threshold to identify the onset of seawater / saltwater intrusion and a novel categorization of groundwater in coastal aquifers. J Hydrol 653:132775. https://doi.org/10.1016/j.jhydrol.2025.132775
36. Krieger R.A. (1963) The chemistry of saline waters. Groundwater 1:7–12
37. Shakiba M, Shahsavari MH (2023) Simultaneous effects of normal stress and sand grain size on fluid storativity, transmissibility and structural strength of artificial sandstones. Int J Geomech 23:1–13. https://doi.org/10.1061/IJGNAI.GMENG-7698
38. Shahsavari MH, Shakiba M (2022) An experimental insight into the influence of sand grain size distribution on the petrophysical and Geomechanical properties of artificially made sandstones. J Pet Sci Eng 215:110632. https://doi.org/10.1016/j.petrol.2022.110632
39. Ismail MA, Joer HA, Randolph MF, Meritt A (2002) Cementation of porous materials using calcite. Geotechnique 52:313–324
40. Shahsavari MH, Shakiba M (2022) An experimental insight into the influence of sand grain size distribution on the petrophysical and Geomechanical properties of artificially made sandstones. J Pet Sci Eng 215:110632
41. Shakiba M, Shahsavari MH (2022) Simultaneous effects of normal stress and sand grain size on fluid storativity, transmissibility and structural strength of artificial sandstones, Int. J. Geomech. 23 1–13. https://doi.org/10.1061/IJGNAI/GMENG-7698. In press
42. Raja PB, Munusamy KR, Perumal V, Ibrahim MNM (2022) Characterization of nanomaterial used in nanobioremediation, in: Nano-Bioremediation Fundam. Appl., Elsevier, : pp. 57–83
43. De Windt L, Deneele D, Maubec N (2014) Kinetics of lime/bentonite pozzolanic reactions at 20 and 50 C: batch tests and modeling, Cem. Concr Res 59:34–42
44. Pettauer M, Baldermann A, Eder S, Dietzel M (2024) Hydration of mgo: reaction kinetics and pH control on brucite crystal morphology. https://doi.org/10.1021/acs.cgd.4c00243
45. Taylor P, Evans BW (2010) The serpentinite multisystem revisited: Chrysotile Is Metastable, 37–41
46. Taylor HFW, Famy C, Scrivener KL (2001) Delayed ettringite formation. Cem Concr Res 31(5):683–693. https://doi.org/10.1016/S0008-8846(01)00466-5
47. Meunier A, Clays (2005) Springer Science & Business Media
48. Gartner EM, Young JF, Damidot DA, Jawed I (2002) Hydration of Portland cement. Struct. Perform. Cem. Spon, London, pp 57–113
49. Davidovits J (2008) Chemistry and applications geopolymer institute, inst. Geopolymere. Saint-Quentin, Fr
50. Shahsavari MH, Karbala MM, Iranfar S, Vandeginste V (2022) Martian and lunar sulfur concrete mechanical and chemical properties considering regolith ingredients and sublimation. Constr Build Mater 350:128914
51. Gardolinski JEF (2005) Interlayer grafting and delamination of kaolinite, Kiel, Univ., Diss
52. Liu W, Wang X, Liu W, Wei D, Wang B, Shen Y (2015) Synergistic adsorption of N–dodecyl Ethylenediamine along with polyethylene glycol (PEG) on quartz. Int J Electrochem Sci 10:9310–9323
53. Tanpure S, Ghanwat V, Shinde B, Tanpure K, Lawande S (2022) The eggshell waste transformed green and efficient synthesis of K-Ca (OH) 2 catalyst for room temperature synthesis of Chalcones. Polycycl Aromat Compd 42:1322–1340

54. Matei C, Berger D, Dumbrava A, Radu MD, Gheorghe E (2020) Calcium carbonate as silver carrier in composite materials obtained in green seaweed extract with topical applications. J Sol-Gel Sci Technol 93:315–323
55. Guan W, Ji F, Chen Q, Yan P, Pei L (2013) Synthesis and enhanced phosphate recovery property of porous calcium silicate hydrate using polyethyleneglycol as pore-generation agent. Mater (Basel) 6:2846–2861
56. Zhang H, Liu Q, Wang J, Liu J, Yan H, Jing X, Zhang B (2015) Preparation of magnetic calcium silicate hydrate for the efficient removal of uranium from aqueous systems. Rsc Adv 5:5904–5912
57. McBride MB (1994) Environmental chemistry of soils. Oxford Univ. Press. Inc., New York
58. Xing H, Yang X, Xu C, Ye G (2009) Strength characteristics and mechanisms of salt-rich soil–cement. Eng Geol 103:33–38
59. Estrada-Flores S, Martínez-Luévanos A, Bartolo-Pérez P, García-Cerda LA, Flores-Guia TE (2018) Aguilera-González, facile synthesis of novel calcium silicate hydrated-nylon 6/66 nanocomposites by solution mixing method. RSC Adv 8:41818–41827
60. Ashraf W, Olek J, Atakan V (2015) A comparative study of the reactivity of calcium silicates during hydration and carbonation reactions. 14th int. Congr. Cem. Chem. Beijing, China
61. Ashraf W, Olek J (2016) Carbonation behavior of hydraulic and non-hydraulic calcium silicates: potential of utilizing low-lime calcium silicates in cement-based materials. J Mater Sci 51:6173–6191
62. Ansari A, Ali A, Asif M (2018) Microwave-assisted MgO NP catalyzed one-pot multicomponent synthesis of polysubstituted steroidal pyridines. New J Chem 42:184–197
63. Zahir MH, Rahman MM, Irshad K, Rahman MM (2019) Shape-stabilized phase change materials for solar energy storage: MgO and Mg(OH)2 mixed with polyethylene glycol. Nanomaterials 9:1773
64. Fuchs Y, Linares J, Mellini M (1998) Mössbauer and infrared spectrometry of lizardite-1T from Monte Fico. Elba Phys Chem Min 26:111–115
65. Mellini M, Fuchs Y, Viti C, Lemaire C, Linarès J (2002) Insights into the Antigorite structure from Mossbauer and FTIR spectroscopies. Eur J Mineral 14:97–104
66. Akula P, Little DN (2021) Mineralogical characterization and thermodynamic modeling of synthesized ettringite from Ca-Al-SO4 suspensions, Constr. Build Mater 269:121304
67. Perkins RB, Palmer CD (1999) Solubility of ettringite (Ca6 [Al (OH) 6] 2 (SO4) 3· 26H2O) at 5–75° C, Geochim. Cosmochim Acta 63:1969–1980
68. Seryotkin YV, Sokol EV, Kokh SN, Sharygin VV (2019) Natural bentorite—Cr 3 + derivate of ettringite: determination of crystal structure. Phys Chem Min 46:553–570
69. Dramé H, Beaudoin JJ, Raki L (2007) A comparative study of the volume stability of C–S–H (I) and Portland cement paste in aqueous salt solutions. J Mater Sci 42:6837–6846
70. Oddo JE, Tomson MB (1994) Why scale forms in the oil field and methods to predict it. SPE Prod Facil 9:47–54
71. Ghasemian J, Riahi S, Ayatollahi S, Mokhtari R (2019) Effect of salinity and ion type on formation damage due to inorganic scale deposition and introducing optimum salinity. J Pet Sci Eng 177:270–281
72. Sawdy-Heritage AM, Heritage A, Pel L (2008) A review of salt transport in porous media: assessment methods and salt reduction treatments, in: conf. Salt weather. Build. Stone Sculpt.
73. Myneni SCB, Traina SJ, Logan TJ (1998) Ettringite solubility and geochemistry of the Ca (OH) 2–Al2 (SO4) 3–H2O system at 1 atm pressure and 298 K. Chem Geol 148:1–19
74. Lafay R, Montes-Hernandez G, Janots E, Chiriac R, Findling N, Toche F (2014) Simultaneous precipitation of magnesite and Lizardite from hydrothermal alteration of olivine under high-carbonate alkalinity. Chem Geol 368:63–75
75. Jalilian M, Pourafshary P, Sola BS, Kamari M (2017) Optimization of smart water chemical composition for carbonate rocks through comparison of active cations performance. J Energy Resour Technol 139:62904
76. Huinink HP, Pel L, Michels MvAJ (2002) How ions distribute in a drying porous medium: a simple model. Phys Fluids 14:1389–1395
77. Chen L, He A, Zhao J, Kang Q, Li Z-Y, Carmeliet J, Shikazono N, Tao W-Q (2022) Pore-scale modeling of complex transport phenomena in porous media. Prog Energy Combust Sci 88:100968
78. Liu H-H, Zhang G, Yi Z, Wang Y (2013) A permeability-change relationship in the dryout zone for CO2 injection into saline aquifers. Int J Greenh Gas Control 15:42–47
79. Ott H, Roels SM, De Kloe K (2015) Salt precipitation due to supercritical gas injection: I. Capillary-driven flow in unimodal sandstone. Int J Greenh Gas Control 43:247–255
80. Ott H, Snippe J, de Kloe K (2021) Salt precipitation due to supercritical gas injection: II. Capillary transport in multi porosity rocks. Int J Greenh Gas Control 105:103233
81. Anselmetti FS, Eberli GP (1993) Controls on Sonic velocity in carbonates. Pure Appl Geophys 141:287–323
82. Iranfar S, Karbala MM, Shakiba M, Shahsavari MH (2023) Effects of type and distribution of clay minerals on the physico-chemical and Geomechanical properties of engineered porous rocks. Sci Rep 13:5837. https://doi.org/10.1038/s41598-023-33103-4

Publisher's note